Solvation of Small Disulfonate Anions in Water/Methanol Mixtures Characterized by High-Field Pulse Electron Nuclear Double Resonance and Molecular Dynamics Simulations

Jeannine Heller,[†] Hossam Elgabarty,[‡] Bilin Zhuang,[†] Daniel Sebastiani,*,[‡] and Dariush Hinderberger*,[†]

Max Planck Institute for Polymer Research, Ackermannweg 10, 55128 Mainz, Germany, and Department of Physics, Freie Universität Berlin, Arnimallee 14, 14195 Berlin, Germany

Received: October 29, 2009; Revised Manuscript Received: April 23, 2010

The solvation of Fremy's salt, the paramagnetic nitrosodisulfonate anion $ON(SO_3^-)_2$, in binary solvent mixtures was investigated by means of pulse (Mims- and Davies-type) electron nuclear double resonance (ENDOR) spectroscopy and molecular dynamics (MD) simulations. ^1H and ^2H pulse ENDOR measurements were performed on small Fremy's salt radicals in isotope-substituted solvent mixtures of methanol and water in frozen solution. We were able to obtain well-resolved, orientation-selective, high-field/high-frequency pulse ENDOR spectra of *methyl* protons from the alcohol moiety and *exchangeable* protons from the alcohol-hydroxyl group and water. In the studied solvent systems (volume ratio $v/v = 30{:}70, 50{:}50, 70{:}30$), the solvation of 2.5 mM Fremy's salt by methyl protons was found to be almost identical. From the analysis of the dependence of pulse ENDOR spectra on the observer field position and spectral simulations, we obtained the principal components of the hyperfine coupling (hfc) tensor for each class of protons. The combination of Mims- and Davies-type pulse ENDOR measurements was necessary to obtain blind spot free information on hfc that spans a broad range of 0.25−6 MHz. Using the point-dipole approximation, the dipolar hfc component yields a prominent electron−nuclear distance of 3.5 Å between Fremy's salt and methyl protons, which was found along the molecular *z*-axis (perpendicular to the approximate plane spanned by $ON(S)_2$) of the probe molecule. Exchangeable protons were found to be distributed nearly isotropically, forming a hydrogen-bonded network around the sulfonate groups. The distribution of exchangeable and methyl protons found in MD simulations is in very good agreement with the pulse ENDOR results, and we find that solvation is dominated by an interplay of H-bond (electrostatic) interactions and steric properties. The elucidation of the microscopic solvation of a small probe molecule in binary solvent mixtures represents the first step for understanding the interactions in more complex biochemical systems. In particular, this includes the potential perturbation of the H-bond network due to the presence of a spin probe or other polar molecules.

1. Introduction

The understanding of ion solvation in multicomponent systems is crucial for many chemical reactions,[1] in electrochemistry,[2] and for understanding the role of ions in biological systems. In solution, ions interact with one another and with solvent molecules. In mixed solvents, the solute may interact specifically with one solvent species, thus changing the composition of solvation shell from that of the bulk. This phenomenon of "preferential solvation"[3] has been studied extensively during the past years by applying experimental[4−7] and theroretical[8−11] methods.

The study of solvation of paramagnetic ions with methods of electron paramagnetic resonance (EPR) spectroscopy was established more than 20 years ago, in particular for transition metal ions.[12−14] The solvation shell of the VO^{2+} ion was one of the first examined with continuous wave (CW) electron nuclear double resonance (ENDOR) spectroscopy.[13,15,16] These measurements were restricted to paramagnetic ions that exhibit large *g*-anisotropy even at low magnetic field. Today, modern spectrometers operating at higher magnetic field offer the possibility to study systems with very small *g*-anisotropies like nitroxides. Nitroxides are compounds containing the

$$>N\overset{\bullet}{-}O$$

group which has an unpaired electron located in a $2p\pi^*$ molecular orbital of the NO group (two-center, three-electron bonding). EPR spectra are very sensitive to environmental changes like polarity of the solvents, and especially the A_{zz} principal value of the nitrogen hyperfine tensor and the g_{xx} principal value of the **g**-tensor were found to depend on the local dielectric medium and hydrogen bonding to the N−O group, which allows their use in biochemical research of diamagnetic proteins in combination with site-directed spin labeling.[17,18] Although in such EPR measurements binary solvent mixtures are usually employed because of the need for a cryoprotectant (pulsed measurements are usually performed at cryogenic temperatures), the effect of the nitroxide solvation is only rarely discussed. In this study, we chose Fremy's salt as a simple model ion to investigate its solvation in binary water−organic solvent mixtures.

In magnetic resonance spectroscopy, Fremy's salt (FS, potassium nitrosodisulfonate $ON(SO_3^-)_2$) is a well-known and frequently used free radical. It is used as an EPR standard for

* To whom correspondence should be addressed. E-mail: dariush.hinderberger@mpip-mainz.mpg.de. Tel.: +49 6131 379 126. Fax: +49 6131 379 100. E-mail: daniel.sebastiani@fu-berlin.de. Tel.: +49 30 838 53037.
† Max Planck Institute for Polymer Research.
‡ Freie Universität Berlin.

g-value determination and radical quantitation[19] and, due to the sensitivity of its ^{14}N hyperfine splitting toward temperature, as an internal thermometer in solution EPR.[20] As an oxidizing agent, it is widely used as a model for reactive oxygen species (ROS).[21,22] Recently, the narrow line shape of FS—resulting from the lack of unresolved ^{1}H hyperfine splittings—has been utilized in new applications; e.g., it could be used to study the distribution of counterions in polyelectrolyte systems in solution[23–25] and for NMR signal enhancement by dynamic nuclear polarization (DNP).[26]

We chose methanol—water mixtures as binary solvent mixtures as they represent the simplest case of an aqueous solution with a cryoprotectant (usually a higher alcohol like ethylene glycol or glycerol is used). Furthermore, such mixtures are used as reaction media in organic synthesis,[1] and it was found that a higher methanol content is responsible for enhanced kinetics in some oxidation reactions, indicating an important potential effect of preferential solvation.[27]

In this study, we use Mims[28] and Davies[29] pulse ENDOR experiments to study the solvation of FS in methanol—water mixtures at high magnetic field *B*/high frequency (W-Band, *B* ∼ 3350 mT, microwave frequency ∼94.5 GHz). Our main tool to achieve selectivity concerning the solvation of the small probe molecule is the selective isotope modification of either *methyl* protons ($-CH_3$) of methanol or *exchangeable* protons from the alcohol-hydroxyl group and water. Working at high magnetic field has two advantages: (i) the **g**- and **A**-matrices are fully resolved in the nitroxide EPR spectrum, thus allowing orientation-resolved EPR and ENDOR, and (ii) the Larmor frequency of ^{1}H is about 149 MHz and of ^{2}H is 23 MHz, hence they are well separated from each other. Together, this allows independent and molecular orientation-dependent monitoring of either proton—electron hyperfine (hf) interactions or deuteron—electron hf interactions in one ENDOR experiment and with this a selective "switching off" of one chemical proton species (exchangeable or methyl protons). In an [1]H-ENDOR spectrum of the CH_3OD-D_2O mixture, only methyl protons contribute to the ENDOR signal, while in an [2]H-ENDOR measurement of the same sample only exchangeable protons that are hyperfine coupled to FS are monitored. Neglecting the small isotope effect of deuteration,[30,31] combining high-field ENDOR and selective isotope substitution allows a more simplified data interpretation. The qualitative comparison of the EPR spectroscopic findings with the picture of solvation derived from our classical molecular dynamics simulations gives unique insights into the solvation shell of the small disulfonate anions in water/methanol solution.

2. Experimental Section

2.1. Samples. Fremy's salt, FS ($K_2[ON(SO_3)_2]$ potassium nitrosodisulfonate, ICN Biomedicals Inc.), was used without purification. D_2O (99.9%), methanol-d_1 (CAS 1455-13-6, CH_3OD, 99.5%), methanol-d_3 (CAS 1849-29-2, CD_3OH, 99.8%), and methanol-d_4 (CAS 811-98-3, CD_4O, 99%) were obtained from Aldrich. All solutions were prepared at ambient conditions without the use of inert gas. Fremy's salt undergoes decomposition in the solid state[32] and in aqueous[33] as well as nonaqueous[34] solution. The optimum solution pH for FS stability is between 9 and 10,[33] and therefore solutions are usually basified with either potassium hydroxide (KOH),[35] carbonate (K_2CO_3),[36] or hydrogen carbonate ($KHCO_3$).[37] The two latter have the advantage of not only producing alkaline solutions but also buffering these solutions. Nevertheless, we explicitly used KOH solutions to adjust the pH to exclude the introduction of a new ion species (carbonate ions) into the system. In all samples, we

TABLE 1: Investigated Samples of 2.5 mM Fremy's Salt in Methanol—Water Mixtures[a]

solvent	V_M:V_W	x_M	w_M	ε	η [mPa s]
CH_3OD:D_2O	30:70	0.15	0.24	76	1.47
CH_3OD:D_2O	50:50	0.31	0.42	65	1.57
CH_3OD:D_2O	70:30	0.49	0.63	53	1.34
CD_3OH:H_2O	50:50	0.31	0.46	65	1.57
CD_3OD:D_2O	50:50	0.31	0.44	65	1.57
CH_3OH:H_2O	50:50	0.31	0.44	65	1.57

[a] The static dielectric constant ε (adapted from ref 39) and the absolute viscosity η (adapted from ref 38) of the solvent mixtures are listed for binary solvent mixtures at *T* = 298.15 K. V_M, V_W: Volume ratio for methanol and water. x_M, w_M: Molar ratio and weight ratio of methanol.

used a KOH concentration of $c_{KOH} = 9.8 \times 10^{-4}$ M and FS concentrations of 2.5 mM.

Stock solutions of 10 mM FS in Milli-Q water (Millipore) and D_2O were prepared, and a solution of 2 M KOH solution was added. The obtained solutions were diluted to 5 mM FS concentration and stored at −18 °C. From the aqueous solutions, the alcohol/water mixtures were prepared by adding the according volume of methanol. Volume ratios of methanol—water *v*/*v* = 30:70, 50:50, and 70:30 were prepared (Table 1), corresponding to a methanol molar ratio of x_M = 0.16, 0.31, and 0.49, respectively. Solutions with higher methanol ratios ($x_M > 0.5$) were not prepared due to reduced solubility of FS in these mixtures. Lower concentrations ($x_M < 0.16$) could not be tested as they do not form glassy solutions upon freezing within our experimental setup. In purely aqueous frozen solutions, local crystallization will change the solvation characteristics and complicate data analysis and is therefore not desired. All experiments are analyzed under the assumption that the shock frozen solutions with methanol as cryoprotectant represent the solvation characteristics at room temperature (or more precisely at the glass transition temperature). This assumption is essential for the comparison of the ENDOR data and the MD simulations.

The following solvent mixtures were used to distinguish between exchangeable protons arising from hydroxyl groups and water and nonexchangeable protons from the methyl group: H_2O/CH_3OH, i.e., the completely protonated mixture; D_2O/ CD_3OD, i.e., the completely deuterated mixture; D_2O/CH_3OD, where only the exchangeable hydrogens are replaced by ^{2}H; and H_2O/CD_3OH, where the nonexchangeable hydrogens are deuterated. The prepared samples are listed in Table 1 together with some properties of the respective pure methanol—water mixtures. Both dielectric constant ε and viscosity η are highly temperature dependent and are only shown for ambient conditions, under which the samples were prepared (*T* ∼ 298 K). The viscosity of pure methanol—water mixtures reaches a maximum at a methanol molar ratio of approximately x_M ∼ 0.29.[38]

2.2. EPR Spectroscopy. *Instrumentation.* W-band measurements were performed on a BRUKER Elexsys E680 spectrometer using a Bruker EN 660-1021 H Tera Flex ENDOR-resonator. The resonator dip was broad enough that further overcoupling was not needed. All measurements were performed at 20 K with liquid helium cooling by an Oxford CF935 cryostat with an Oxford ITC4 temperature controller. Samples were loaded with a Hamilton syringe into 0.7 mm inner diameter homemade CFQ-quartz capillaries to a height of about 3 mm and inserted into the resonator at 50 K and then cooled to 20 K.

Orientation Selection. EPR spectra of nitroxides in frozen solutions result from superposition of EPR signals from all
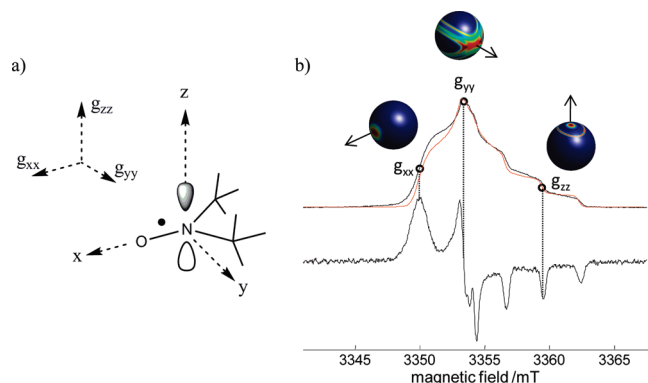
Figure 1. (a) Nitroxide group and its molecular coordinate axis system with the *x*-axes along the NO bond and *z*-axes along the 2p$_\pi$ orbital. The **g**-tensor principal axes system coincides with the molecular axes and the hyperfine tensor coordinate system.[40] (b) Upper: field-swept, echo-detected EPR spectrum of 2.5 mM Fremy's salt in CH_3OD/D_2O with a volume ratio of $v/v = 70:30$, recorded at 94.18 GHz and 20 K. The pulse sequence was $\pi/2$-τ-π-τ-echo, with $t_{\pi/2} = 48$ ns, $t_\pi = 96$ ns, and $\tau = 300$ ns. Lower: The pseudomodulated spectrum calculated with a modulation amplitude of 0.25 mT from the absorption spectrum. The dotted lines indicate the position of the nitroxide principal axis components as shown in the left scheme. Circles indicate observer field positions B_{ENDOR} used for ENDOR measurements. The red spectrum shows the rigid-limit EPR spectrum simulation performed with a rhombic **g**-tensor ($g_{zz} < g_{yy} < g_{xx}$) and a nearly axial **A**-tensor. The unit spheres show the representation of orientation selections for the field positions underlying the simulations of the ENDOR spectra.

molecular orientations with respect to the outer magnetic field. Depending on the magnitude of the magnetic field B_0, the *g*-anisotropy, and the inhomogeneous line width due to unresolved hf couplings, each field position in the EPR spectrum represents a specific manifold of relative molecular orientations from the entire orientation distribution. Going from conventional X- (~9.4 GHz) to W-band (~94.5 GHz) frequencies, the increase of the Zeeman energy, which is proportional to the static external magnetic field B_0, leads to a higher spectral resolution in the EPR spectrum. In particular, for nitroxides which have only small *g*-anisotropies (in the range of 10^{-3}–10^{-4}), the respective increase of B_0 to ~3400 mT is necessary to resolve the **g**-tensor principal values.[40] This is not yet possible at the X-band and only partially achieved at intermediate frequencies (e.g., Q-band, 35 GHz). If the *g*-anisotropy is larger than the hyperfine interaction (as is the case for nitroxides at the W-band), specific turning points in the spectrum can be used to select certain orientations of a radical with respect to the magnetic field. From these magnetic field positions, "single-crystal-like" ENDOR spectra can be obtained equivalent to those from oriented single crystals, and hf tensors can be elucidated with respect to the **g**-tensor principal axes system. This is commonly known as "orientation-selection" or "angle-selection"[41] and was first introduced in 1970 by Rist and Hyde.[42]

For nitroxides, the common right-hand Cartesian molecular frame is chosen, such that the *x*-axis coincides with the direction of the N−O bond and the *z*-axis is directed along the long axis of the singly occupied molecular orbital (SOMO), simplified as a 2p orbital of nitrogen (Figure 1a). Assuming full *g*-resolution, and setting the laboratory magnetic field B_{ENDOR} to the low-field turning point in the EPR spectrum of a frozen solution, a single orientation can be selected such that B_{ENDOR} is aligned parallel to the N−O bond of the nitroxide. At the high-field turning point, only those orientations are selected, for which the unique axis of the SOMO is parallel to the outer

magnetic field. At intermediate magnetic field positions, a well-defined set of orientations is selected, and the ENDOR pattern is in general more complex than a single-crystal-like spectrum.[43,44] Due to the symmetry of the SOMO, its molecular frame coincides with the principal axis of both, the **g**- and the **A**-tensors.[40] The subsequent analysis of the hyperfine couplings assumes colinearity of the **g**-tensor and hyperfine-tensor frames, which is known to be a viable approximation in nitroxide radicals in general and has been shown for Fremy's salt, too.[24]

Pulse EPR and ENDOR Experiments. The field-swept, electron spin echo (ESE) detected EPR spectra were recorded by integrating over the echoes created with the pulse sequence $\pi/2$-τ-$\pi/2$-echo, with the pulse lengths $t_{\pi/2} = 48$ ns, $t_\pi = 96$ ns, and an interpulse delay of $\tau = 300$ ns. From echo-detected spectra, the characteristic points for ENDOR measurements were assigned as shown in Figure 1a. ^{1}H and ^{2}H ENDOR spectra were recorded using the Mims three-pulse scheme ($\pi/2$-τ-$\pi/2$-T-$\pi/2$),[28] with the radiofrequency (RF) pulse applied during time T. A $\pi/2$ pulse length of 48 ns was used. Since Mims-type ENDOR spectra are hampered by blind spots depending on the pulse interval τ, measurements for different values of τ were performed. For ^{1}H measurements, typical values for τ were 172 or 200 ns, for ^{2}H 400−600 ns. The RF pulse length varied for ^{1}H and ^{2}H nuclei and was optimized for the studied nucleus. A typical value for ^{1}H was 20 μs. The RF was swept from 20 to 24 MHz for detection of deuteron hf couplings and from 139 to 147 MHz for proton hf couplings. The Davies ENDOR sequence[29] π-T-$\pi/2$-τ-π-echo was used to record ^{1}H spectra. The inversion π pulse was 200 ns. A radio frequency pulse length of 20 μs was applied during the time T. In the detection sequence ($\pi/2$-τ-π-echo), pulse lengths of $t_{\pi/2} = 200$ ns and $t_\pi = 400$ ns were used with an interpulse delay of $\tau = 548$ ns. The signal was accumulated over 2−5 h for the *x*- and *y*-position and at least 14 h for the *z*-position (due to the weak signal intensity, see Figure 1a).

Mims ENDOR was recorded for both proton species (methyl and exchangeable protons) and both isotopes (^{1}H and ^{2}H). Davies ENDOR was recorded only for the ^{1}H isotope for both proton species since the small deuterium couplings (~2 MHz) and weak signal intensities cannot be properly detected by the Davies ENDOR sequence.[45]

2.3. Spectral Analysis. *Spin Hamiltonian.* The stationary Hamiltonian describes the time-independent spin-interaction energies and is given for the interaction of an $S = 1/2$ electron spin coupled to i nuclei by[45]

$$H = \mu_B \mathbf{B}_0 \mathbf{g} \mathbf{S} + h \sum_i \mathbf{S} \mathbf{A}_i \mathbf{I}_i - \mu_N \sum_i g_N \mathbf{I}_i \mathbf{B}_0 + \sum_i \mathbf{I}_i \mathbf{Q}_i \mathbf{I}_i \tag{1}$$

The first term describes the electron Zeeman interaction, the second term the hyperfine interactions, the third term the nuclear Zeeman interactions, and the last term the nuclear quadrupole interactions (for nuclei with $I > 1/2$, e.g., ^{2}H). The terms are ordered according to their relative magnitude. $\mathbf{A}_i$ and $\mathbf{Q}_i$ denote the hyperfine (hf) and quadrupolar tensors, μ_B and μ_N the Bohr and nuclear magnetons, and $\mathbf{S}$ and $\mathbf{I}$ the electron and nuclear spin operator. $\mathbf{g}$ is the **g**-interaction matrix and g_N the nuclear *g*-factor, respectively. To first order, the last two terms do not contribute to the EPR spectrum. At low magnetic field (X-band 9.5 GHz), the powder pattern is dominated by the anisotropy of the field-independent hyperfine term. Therefore, the *x*- and *y*-orientations of the nitroxide **g**-tensor (Figure 1) are indistinguishable. At ten times higher magnetic field (W-band 94.5

GHz), the anisotropy of the Zeeman term and all principal axis orientations are resolved.

The hf tensor **A** consists of an isotropic part, a_{iso}, and a dipolar part T and has the principal components, $\mathbf{A} = [A_{xx}A_{yy}A_{zz}]$. If the anisotropic hyperfine coupling can be described by the point-dipole approximation, the principal values of **A** become $A_{xx} = A_{yy} = A_{\perp} = -T + a_{iso}$ and $A_{zz} = 2T + a_{iso}$, and $T = [\mu_0/(4\pi\hbar)]g\mu_Bg_N\mu_N(1/r^5)$ with r being the electron−nuclear distance.

The first-order ENDOR transition frequencies (no quadrupolar coupling) for a nucleus N are given by

$$\nu_\pm = \left| \nu^N \pm \frac{A^N}{2} \right| \qquad (2)$$

where $\nu^N = g_N\mu_NB_0/h$ is the nuclear Larmor frequency and A^N is the orientation-dependent hyperfine coupling constant. For protons at a magnetic field of ∼3500 mT, $\nu^H > A^H/2$, and the ENDOR spectrum is a doublet centered at the proton Larmor frequency ν^H and split by A^H. For nuclei $I > 1/2$, the nuclear frequencies additionally depend on the nuclear quadrupole interaction Q.

The anisotropic hf and quadrupolar interactions tilt the quantization axis of a nuclear spin. The criterion for the magnetic field at which the effects of tilting can be neglected is $g_N\mu_NB_0 > T_{II}$, Q_{II} and is usually valid for nitroxides at 95 GHz.

In the case of axial symmetry of the hf interaction tensor, the distance dependence of the perpendicular component T is given by eq 3

$$T = \frac{\mu_0\rho}{4\pi\hbar} \cdot \frac{g\mu_Bg_N\mu_N}{r^3} \qquad (3)$$

where $\rho = |\psi(0)|^2$ is the electron spin density.[45]

Spectral simulations were performed with the program package EasySpin 3.0.0.[46] Line positions and intensities were calculated by exact matrix diagonalization of the respective spin Hamiltonian. The **g**-tensor principal values and ^{14}N hf coupling were obtained from simulation of the powder EPR spectrum (including all orientations). The ENDOR transition frequencies were only calculated for the set of molecules that contribute to the ENDOR spectrum at the observer field position B_{ENDOR} and that are excited within a Gaussian EPR line width calculated from the pulse length t_p of the first pulse that was applied in the ENDOR experiment. The full width at half-maximum (fwhm) of this Gaussian line was determined by $2/t_p$. In all simulations, the line widths (Gaussian, Lorentzian, or Voigtian) were set empirically to fit the experimental spectra. Line widths and relative amplitudes were not determined analytically in ENDOR spectra.

Data Treatment. All spectra were background-corrected using a home-written MATLAB program, by subtracting a first-order polynomial fit from the first and last 15% of the data points (baseline regions). Mims ENDOR signals were inverted; all types of ENDOR spectra were centered around the corresponding Larmor frequency; and spectra were normalized either by their maximum or relative to the intensity of their position B_{ENDOR} in the ESE-detected EPR spectrum.

2.4. Molecular Dynamics Simulations. A Fremy's salt anion was charge neutralized by two potassium cations. The whole system was solvated with 492 methanol and 1104 water molecules in a cubic box of side length 40 Å, which corresponds to a water:methanol volume ratio of 1:1. A classical molecular

dynamics (MD) run was performed under periodic boundary conditions using the Gromacs simulation package.[47] The box was kept at a temperature of 300 K by means of Nose−Hoover thermostats[48,49] with a coupling constant of 0.1 ps. The total simulation time was 10 ns, using a time step of 0.5 fs. The particle-mesh Ewald (PME) algorithm[50,51] was used for long-range electrostatics interactions, and a cutoff of 9 A was employed for the Lennard-Jones interactions with analytic long-range dispersion corrections for energy.

The OPLS force field[52] was used for the alcohol molecules, together with the TIP3P water model.[53] To obtain force field parameters for the FS anion, a scan of the potential energy surface was performed in Gaussian 03 at the B3LYP/6-31+G* level.[54] We scanned each of the N−O, N−S, and S−O bond stretching modes, as well as all the bond angles in the molecule. Harmonic stretching and bending force constants were obtained by parabolic fitting of the obtained potential energy profiles. Standard values for the dihedral potentials of the FS anion were extracted from the OPLS force field. Partial atomic charges were obtained by fitting to the molecular electrostatic potential (B3LYP/6-31+G*) using the RESP method.[55]

To mimic the shock freezing treatment (as done in the EPR experiments), snapshots were taken, each 50 ps from the trajectory. Each snapshot was annealed down slowly to 250 K over a time period of 200 ps and then down to 50 K in another 100 ps.

3. Results

Electron Spin Echo (ESE)-Detected EPR Spectra. All ESE-detected EPR spectra exhibit the typical nitroxide powder pattern line shape expected for a dilute distribution of nitroxide radicals. The spectra show full resolution of the **g**-tensor and its elements g_{xx}, g_{yy}, and g_{zz} with a total width of 15 mT. Figure 1b shows a representative ESE-detected EPR spectrum (black). The spectral simulation is plotted in red. The spheres were calculated from the simulated spectra and represent the selected orientations for the field positions marked with a circle and hence the orientations selected in ENDOR experiments at these positions. As mentioned above, only at the turning points (g_{xx} and g_{zz}) a finite solid angle of molecular orientation is selected, whereas at the intermediate position and g_{yy} a well-defined set of orientations contribute to the ENDOR signal. In particular, at the maximum of the EPR spectrum molecular orientations that have x- and z-contributions also contribute to the ENDOR spectrum.

The best simulations were obtained by introducing an anisotropic line width that can model small effects such as unresolved hyperfine splitting or g- or A-strain. The EPR parameters found from simulating the experimental EPR spectra are $g = [2.00844, 2.00625, 2.00285] \pm 2 \times 10^{-5}$ and $A = [0.41, 0.40, 2.86]$ mT for the principal values of the **g**- and **A**-tensor, respectively. The errors for **A**-tensor components are ±0.1 mT for the x-, ±0.02 mT for the y-, and ±0.01 mT for the z-component. A Voigtian-type line width is found with a fwhm of 0.3 mT (Gaussian part) and 0.09 mT (Lorentzian part). In solid state EPR spectra, homogeneous line broadening (T_2-broadening) is usually negligible. Thus, the slight mismatch between simulation with a purely Gaussian line and experiment might be due to nuclear relaxation effects. An orientation-dependent phenomenological broadening of 15−25 MHz is found along x, 8−17 MHz along y, and 8−19 MHz along z, in which the magnitude follows the order $x > z > y$ for all samples. Due to this broadening, the error for the x-component of the **A**-tensor is much higher than for the other components. Even

Solvation of Fremy Salt in Water−Methanol Mixtures

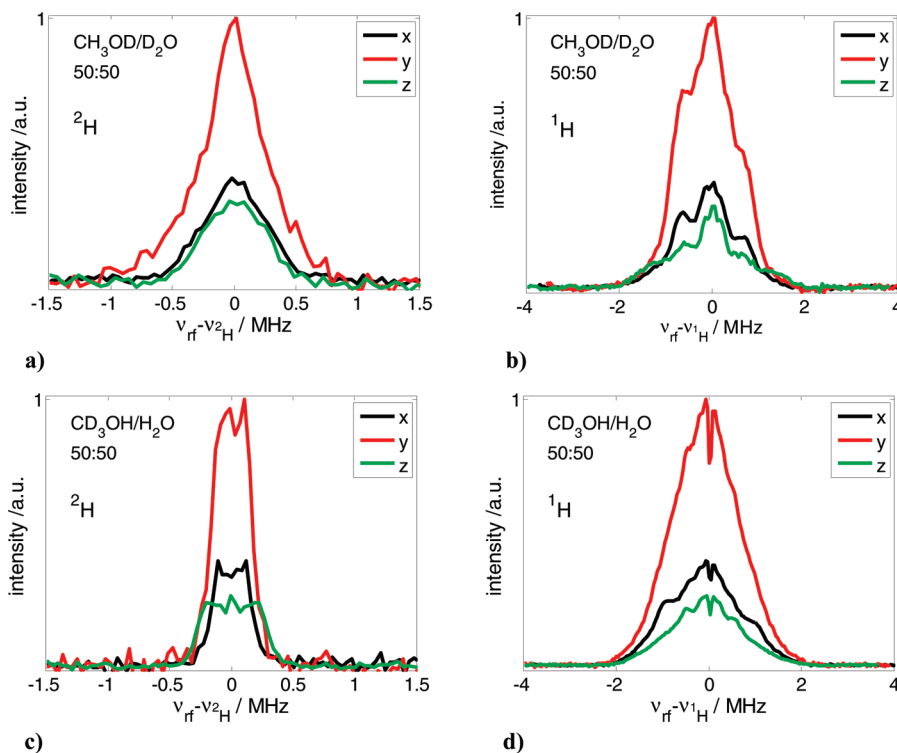*J. Phys. Chem. B, Vol. 114, No. 22, 2010* **7433**

Figure 2. Orientation-selective Mims-ENDOR spectra of 2.5 mM Fremy's salt in frozen solution. (a), (b) ^{2}H spectra and ^{1}H spectra of the solvent mixture CH_3OD/D_2O (v/v = 50:50). (c), (d) ^{2}H spectra and ^{1}H spectra of the solvent mixture CD_3OH/H_2O (v/v = 50:50). Spectra were recorded from the low-field turning point g_{xx} (black) to the high-field turning point g_{zz} (green) of the EPR spectrum. Experimental parameters: T = 20 K; MW $\pi/2$ pulse, 48 ns; τ for ^{1}H, 172 ns (b), 200 ns (d). τ for ^{2}H: 400 ns (a), 600 ns (c). RF π pulse, 20 μs for ^{1}H and 35 μs for ^{2}H. The spectra are normalized relative to the EPR spectral intensity at their field position B_{ENDOR}.

with this additional broadening, the low-field flank of the simulated spectra never reaches the experimental spectrum. Better results are obtained by simulation of two species with different g_{xx} value (with the other parameters identical). This could be indicative of the existence of some FS NO-groups, which participate in hydrogen-bonded structures, as the g_{xx} value is known to be sensitive to the formation of hydrogen bonds. At this point we refrain from a more detailed analysis of this observation and show the simulated spectrum in Figure 1b (red) that was calculated with a single species.

Notably, the line widths in completely deuterated solvent and in completely protonated solvent differ only slightly from each other, indicating that the broadening due to unresolved ^{1}H hyperfine couplings to solvent hydrogens is negligible in low-temperature ESE-detected EPR spectra. No difference in the A_{zz} value was observed between the deuterated and protonated sample mixture with a solvent ratio of v/v = 50:50 (ε = 65). Comparing the solvent mixtures with higher (70 vol %, ε = 53) and lower (30 vol %, ε = 77) amounts of methanol, no variation of A_{zz} with solvent polarity is observed either. The low-field region of the ESE spectrum of the water-rich solvent mixture (70 vol % H_2O) is broadened, and a slightly higher g_{xx}-value (increased by 5×10^{-5}) is found. The best simulation for this sample is given after introduction of a second species with pronounced higher g_{xx}-value (4×10^{-4}). No differences for the g_{xx}-values of the mixtures with 50 vol % and 70 vol % methanol are observed, which indicates that the hydrogen bonding to NO is similar in these two solvent mixtures.

Mims ENDOR Measurements. The following color code is used in all figures and for all spectra: black marks the x-, red the y-, and green the z-direction in the nitroxide reference frame (Figure 1a). In Mims ENDOR, the intensity is modulated by a periodic dependence of the interpulse spacing τ, given by I_{ENDOR}

$\sim 1 - \cos(2\pi A \tau)$,[45] where τ denotes the pulse spacing between the last two $\pi/2$ pulses. An increased value for τ led to a symmetric narrowing of the spectra from both sides affecting mostly the width of the broadest coupling. This was most pronounced in ^{2}H measurements since large τ-values have been used for their detection (600 ns). Attempts to measure ^{2}H ENDOR with shorter τ values suffered from poor signal-to-noise (S/N) ratio. Hence, analysis of ^{2}H Mims ENDOR spectra is only given in a qualitative way.

In all Mims ENDOR spectra an intense peak is observed centered around the larmor frequency of the respective nucleus. Such matrix lines in ENDOR spectra are due to very weak hyperfine interactions of the unpaired electron with distant matrix nuclei and originate from simultaneous inversion of a large number of nuclear spins by the rf pulse.[56] The analysis of weakly coupled protons in the solvation shell is complicated, as these resonances overlap with the matrix peak. The largest hyperfine splitting observed in Mims-ENDOR spectra is ~4.2 MHz (at ±2.1 MHz) for ^{1}H and ~0.84 MHz (at ±0.42 MHz) for ^{2}H, both of which are still quite small (in particular, when compared to the Davies ENDOR results presented later). No further splittings with larger hf couplings were observed in spectra recorded with wider radio frequency sweep ranges.

For the solvent mixture CH_3OD/D_2O, other volume ratios with higher methanol (70 vol %, ε = 53) and lower (30 vol %, ε = 77) content were prepared. Their ^{1}H-Mims ENDOR spectra exhibit identical line shapes and only slight intensity variations for the different positions x, y, and z as compared to the sample with 50 vol % methanol in Figure 2 (data not shown). The mixture with low methanol content gave only poor S/N ratio in the ENDOR experiments but shows also the same trend upon variation of the observer field position.
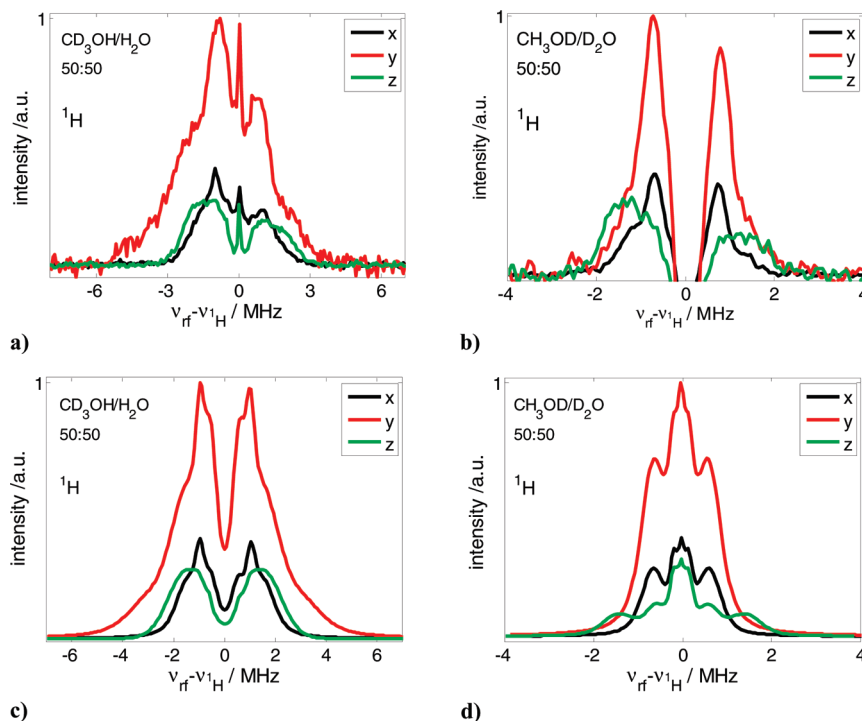
Figure 3. W-Band [1]H Davies ENDOR spectra of 2.5 mM Fremy's salt in frozen solution for the solvent mixture (a) CD_3OH/H_2O and (b) CH_3OD/D_2O. Both mixtures contain 50 vol % methanol. The spectra were recorded at field positions corresponding to the canonical values of the **g**-tensor g_{xx} (black), g_{yy} (red), and g_{zz} (green), as defined in Figure 1a. Experimental parameters: $T = 20$ K; MW inversion pulse, $t_\pi = 200$ ns; RF, $t_\pi = 20$ μs; MW detection pulse, $t_{\pi/2} = 200$ ns; $\tau = 548$ ns. (c) ^{1}H ENDOR simulation of exchangeable protons in the sample mixture CD_3OH/H_2O. (d) Simulation of methyl protons in the mixture CH_3OD/D_2O. The spectra are normalized relative to the EPR spectral intensity at their field position B_{ENDOR}.

Davies ENDOR Measurements. Davies ENDOR spectra were only recorded for the ^{1}H isotope and shown in Figure 3 for the solvent mixtures with equal volume ratios $v/v = 50:50$ of methanol and water. Due to the weaker signal intensity (as compared to Mims ENDOR), it was impossible to record [2]H Davies ENDOR spectra within reasonable measurement time.

In Figure 3a, the orientation-dependent [1]H-Davies ENDOR spectra for the solvent mixture CD_3OH/H_2O are shown. Along the molecular x-axis (black), the peaks at ∼±1.1 MHz (splitting = 2.2 MHz) are the most prominent features in the spectrum. When changing the field position B_{ENDOR} to the molecular y-axis (red), this coupling is still observed, but a second one at ∼±2.5 MHz (splitting = 5 MHz) and a very broad flank that extends out to ∼±6 MHz appear, too. When changing the field B_{ENDOR} to match the molecular z-orientation, the broad flank disappears again, and the peaks at ∼±2.5 MHz grow in intensity to now match the intensity of the peaks from the smallest splitting.

Indications of the larger couplings of exchangeable hydrogens found along the molecular y-position in Davies ENDOR spectra are already found in the [2]H Mims ENDOR spectrum of the mixture CH_3OD/D_2O (Figure 2a, red line), but the poor S/N ratio does not allow as precise an assignment as in the Davies ENDOR case.

The situation is clearly different for the methyl protons. In this case (Figure 3b), the proton hyperfine couplings along the molecular x- and y-directions are almost identical (a coupling of less than 2 MHz with peaks at ±1 MHz), while a larger, relatively broad hf coupling grows in intensity when measuring along the molecular z-direction (splitting range of 2.5−4 MHz, the broad peaks are centered at ±1.5 MHz). The spectra in Figure 3b suffer from a blind spot around the Larmor frequency, which makes it impossible to analyze small hf couplings. Note

that this blind spot cannot fully explain the signal in Figure 3b turning negative. At this point, we refrain from interpreting which other effects may contribute to this observation that hampers analysis of small hf couplings in these Davies ENDOR spectra. In fact, the [1]H Davies ENDOR spectra (Figure 3b) of the solvent mixture CH_3OD/D_2O qualitatively show the same features as the corresponding Mims ENDOR spectra (Figure 2b); however, Davies ENDOR spectra suffer from a "central" blind spot, while Mims ENDOR spectra suffer from an "outer" blind spot that scales down the largest hf coupling.

This can be seen best at the molecular z-direction (green lines): in the Mims ENDOR spectrum, the outer flank reaches the baseline at ∼±2.0 MHz, while the Davies ENDOR spectra extend to ∼±2.4 MHz. This has direct consequences for the chosen simulation parameters, which are explained in the next section.

ENDOR Simulation. The chemically distinct methyl protons and exchangeable protons could be measured and also simulated individually. Since the [1]H Davies ENDOR spectra for *exchangeable protons* CD_3OH/H_2O (Figure 3a) show more distinct features than the respective Mims ENDOR spectra (Figure 2d), the former was chosen for the simulations. A set of couplings with independent line widths were defined, and the **g**-tensor principal values were taken from the simulated EPR spectrum. For simulation of the ^{1}H ENDOR spectra (Figure 3c), three proton couplings had to be employed to fit the experimental results for the x- and z-position. The matrix peak was neglected (for clarity) but can be included with an isotropic hfc of 10^{-4} MHz. The pronounced feature in the experimental spectrum at the x-orientation is assigned to an hf coupling of $a_{iso}(1) = 1.13$ MHz. The hf couplings $a_{iso}(2) = 2.04$ MHz and $a_{iso}(3) = 3.04$ MHz together describe the flank of the spectra. These couplings were found to be present in all three orientations with

Solvation of Fremy Salt in Water−Methanol Mixtures

J. Phys. Chem. B, Vol. 114, No. 22, 2010 **7435**

different weighting factors. Only the *y*-position could not be simulated successfully with these three hf couplings. As can be seen in the red spectrum in Figure 2a, the very broad shoulder on the left wing requires an additional hf coupling. This was found to be $a_{iso}(6) = 6.20$ MHz. This is by far the strongest coupling found in our measurements and simulations and is only present in this sample mixture and at the molecular *y*-position. This coupling cannot be found in the corresponding ^{1}H Mims ENDOR spectra for the following reason: Assuming the maximum detectable hf coupling in Mims ENDOR to be $A_{max} \sim 1/(2\tau)$,[45] with $\tau = 172$ ns, one gets an approximate maximum detectable hf coupling of $A_{max} \sim 2.9$ MHz for this experiment. Hence, this spectrum suffers from a blind spot region at this value.

The blind spots in the Mims ENDOR spectra mostly affect the outer flank, while the blind spots in the Davies ENDOR spectra affect the central region around the Larmor frequency. Therefore, the simulation of *methyl protons* CH$_3$OD/D$_2$O was performed by combining both spectral features from Davies and Mims ENDOR spectra that do not suffer from the blind spot behavior. This means that the small hf couplings (along the *x*- and *y*-molecular direction) were derived from the ^{1}H Mims ENDOR spectra (Figure 2b, black and red line) and the large hfc that becomes apparent at the molecular *z*-position from the corresponding ^{1}H Davies ENDOR spectrum (Figure 3b, green line). The small hf couplings were found to be nearly isotropic with $a_{iso}(1) = 0.33$ MHz and $a_{iso}(2) = 1.22$ MHz. The larger hf coupling was simulated with a purely anisotropic hfc $\mathbf{A} = \mathbf{T} = [-T, -T, 2T] = [-1.6, -1.6, 3.2]$ MHz ± 0.2 MHz. In a very simplified picture, from the component $T = 1.6$ MHz, a distance of $r = 3.5 \pm 0.1$ Å can be calculated within the point-dipole approximation according to eq 3.[45]

In the ENDOR simulations, it was found that convolution with a Gaussian and a Lorentzian function (Voigtian) with a larger Gaussian fwhm gives the best fits to the experimental spectra, indicating inhomogeneous broadening at all positions. Note that the asymmetry observed in the high-field ENDOR spectra may well stem from the cross- and/or nuclear-relaxation times being longer than the repetition times used in the experiments,[57] which was not considered in the simulation.

Molecular Dynamics Simulation. The solvation of the FS dianion by water and methanol was modeled computationally by means of molecular dynamics simulations using classical force fields. A trajectory of 10 ns duration was generated at a temperature of 300 K to extensively sample the available phase space for this binary solvent mixture. The low-temperature solvation configurations corresponding to the experimental situation were obtained by repeatedly annealing snapshots (200 in total) which were extracted from the 300 K-trajectory at regular intervals.

In the optimized geometry of the FS dianion (Figure 5), a small deviation from a planar hybridization geometry at the nitrogen atom is found with a N−O bond length of 1.283 Å. This is in excellent agreement with the 1.284 Å found by X-ray diffraction.[58]

For ionic solutes, the question of ion pairing in a given solvent is often a matter of concern. Thus, we have monitored the distances between the K$^+$ ions and the dianion in our simulations. In the initial configuration of the system, the dianionic salt was set up as a tight ion pair with the two potassium cations. Within 400 ps, both cations diffused away to a distance of 9 Å from the salt. Only four times during the whole trajectory of 10 ns, a potassium ion diffused back to the dianion. The lifetime of this ion pair never exceeded 100 ps. Thus, ion pairing is

TABLE 2: Calculated Coordination Numbers for the Different Oxygen Species Present in Fremy's Salt

	H$_2$O	HO−CH$_3$
sulfonate−oxygen	1.55	0.47
nitroxide−oxygen	0.62	0.13

unlikely to be a significant issue in this system, especially when considering that our simulated concentration of 25 mM is about 10-fold higher than in experiment. Interestingly, this corresponds well with hyperfine sublevel correlation (HYSCORE) spectroscopy (see Supporting Information) in which hyperfine interaction between the radical and ^{39}K was only observed with larger volume ratios of methanol.

Three distinct types of protons can be analyzed with respect to their interactions with FS: the water protons, the methanol hydroxyl (or alcohol) protons, and the nonexchangeable protons of the hydrophobic methyl group. In principle, all sulfonate oxygens and the nitroxide oxygens in FS can interact as hydrogen bond acceptors with the solvent. Table 2 lists the coordination numbers of the acceptor oxygens of the solvated dianion obtained by integrating the corresponding radial distribution functions (RDF) $g_{OH}(r)$ up to the first minimum. Each of the electron-rich sulfonate oxygens is fully solvated with two hydrogen bonds. In contrast to this, the nitroxide oxygen has a coordination number of only 0.75. This reflects the fact that this oxygen is sterically almost inaccessible, being flanked from both sides with sulfonate groups. This effect is also observable directly from the RDFs (data not shown).

The coordination of the nitroxide oxygen by water protons is almost five times larger than that by methanol, which approximately equals the statistical proton ratio in our simulation box (4.49). The slight preference for water solvation relative to the statistical ratio is probably due to the smaller size of the water molecules, in combination with the mentioned sterical hindrance by the sulfonate groups.

To gain further insight into the solvent structure, we have plotted the angular distribution functions of the different proton species relative to the NO bond in Figure 4. The angle θ is measured between the NO bond axis and the vector pointing from the NO bond center to the solvating proton. For the calculation of these angular distribution functions, solvent protons up to a certain radial cutoff value were considered. The plots in Figure 4 show distribution functions for four different cutoff values.

Regarding the methyl protons, there is a clear preference for $\theta = 90°$ at short distances (up to 3 Å), which corresponds to the direction directly above the molecular plane. There is virtually no density in the direction of the NO bond ($\theta = 0°$) because the size of the methyl group results in a strong sterical hindrance. At 3.5 Å, the angular distribution has reached an almost uniform shape.

Regarding the water protons, only little differences in the amplitudes of the distribution functions at small angles $\theta < 50°$ between cutoff values of 2.5−3.0 Å are observed. This indicates that most of the hydrogen-bonded protons are located at distances shorter than 2.5 Å relative to the NO bond center. At a cutoff of 3.0 Å, a strong peak at $\theta = 60°$ appears, which can be attributed to the solvation of the sulfonate groups. Both these features are also found for the alcoholic hydrogen, except that the distribution function vanishes for very small angles $\theta < 15°$. This again illustrates the sterical hindrance caused by the bulky sulfonates and possibly also the methyl group of methanol.

The picture described above was obtained from analyzing the solvation structure at low temperature. Qualitatively, the
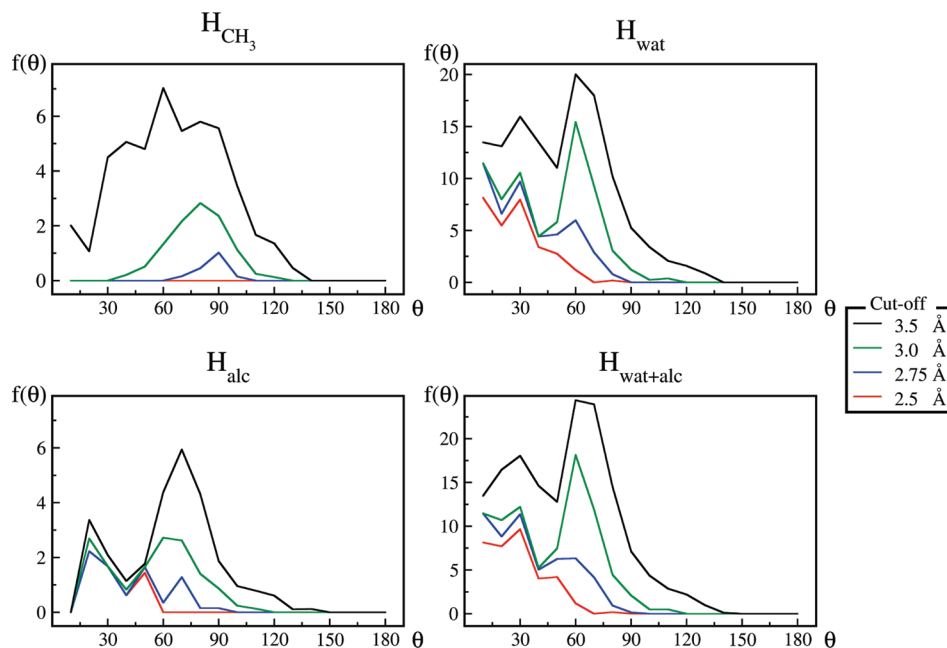
Figure 4. Angular distribution functions of the different proton species relative to the NO bond (water proton, H_{wat}; alcoholic protons, H_{alc}; methyl protons, H_{met}; exchangeable protons, $H_{wat} + H_{alc}$). The angle θ is measured between the NO bond axis and the vector pointing from the NO bond center to the solvating proton. In each plot, protons up to a four different radial cutoff value were considered. Note that up to 3.5 Å, an approach from $\theta = 180$ is sterically impossible for all solvent protons.
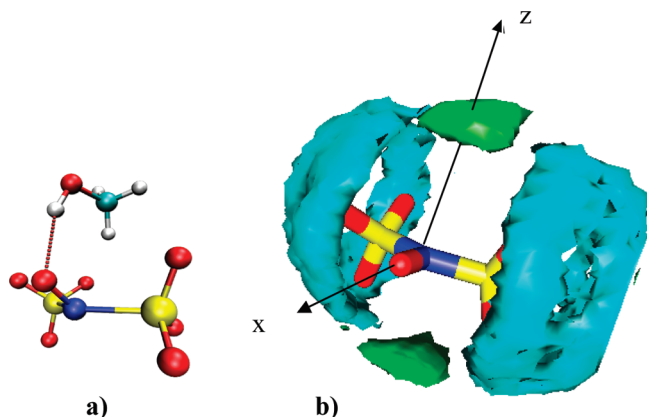

Figure 5. Solvated Fremy's salt. Nitrogen atoms are shown in blue, sulfur atoms in yellow, and oxygen atoms in red. (a) Simulation snapshot from the MD run showing a situation in which one methanol−OH group is hydrogen-bonded to the NO group. (b) Isosurface of the spatial distribution function of the exchangeable protons (cyan) and hydrophobic methyl protons (green) in CH_3OH/H_2O (v/v = 50:50). Along the z-axis of the molecular frame, methyl protons are accumulated, whereas the charged sulfonate groups are strongly hydrogen bonded. A cutoff of 3 Å was used for this picture.

same pattern of solvation exists also at room temperature, and the trend observed in Figure 5—as expected—is slightly more pronounced at low temperature.

The prediction of the actual ENDOR line shape from the simulation data would require the statistical distribution of the **A**-tensors of all protons in proximity of the salt for a large number of annealed snapshots. While this calculation is in principle possible,[59] it requires an extensive additional sampling of our trajectories with quantum-chemical methods, which is beyond the scope of the present work. Here, we restrict ourselves to the geometric distribution of the solvent protons around FS, which is directly available from the MD trajectory. In analogy to this, we do not consider nuclear quantum effects, i.e., the broadening of the proton probability density with respect to the

point particle representation. While there is an ongoing discussion on whether these effects lead to a somewhat more or somewhat less structured hydrogen bonding network,[60−64] we believe that the consequences on the final solvation structure in a complex liquid will not be dramatic.

4. Discussion

Solvation Shell around Fremy's Salt Dianions. When discussing the combined ENDOR and MD results, one should always be aware that the ENDOR measurements depict a complete ensemble of $\sim 10^{15}$ Fremy's salt ions and their solvation shells in the solvent mixtures. Since it is highly unlikely that all FS molecules have the exact same solvation shell, the observable splittings shown in Figures 2 and 3 and their respective simulations only represent a part of the ensemble. Hence, one main source of spectroscopic information is the interpretation of differences between the exchangeable and methyl protons in the ENDOR and MD data.

When a solute ion such as FS is added to a methanol/water mixture, it is reasonable to assume distortion of the hydrogen-bonded network as a response to the existence of the solute ion. Water is a two H-bond donor and two H-bond acceptor, whereas methanol with its single hydroxyl H-atom is only a single H-bond donor and (theoretically) a two H-bond acceptor. When dissolving Fremy's salt, the two sulfonate groups mainly act as hydrogen-bond acceptors, which force some molecules of water into close contact also with the N−O. This can be seen in the [1]H Davies ENDOR spectra for the y-orientation (Figure 3a, red spectrum). Thus, the strongest proton hf coupling with $a_{iso}(6) = 6.20$ MHz can be assigned to hydrogen-bonded water at the sulfonate groups since hydrogen bonding to one of the adjacent sulfonate groups allows protons to approach the NO group closest. The ENDOR measurements are in agreement with the MD simulation that found a coordination number of two for the sulfonate oxygen atoms and the closest approach (down to 2.2 Å) by water and methanol−OH protons to the NO group at small angles (Figure 4a and b). Interestingly, results

Solvation of Fremy Salt in Water−Methanol Mixtures

J. Phys. Chem. B, Vol. 114, No. 22, 2010 **7437**

from Mims and Davies ENDOR measurements along the x-position suggest that the N−O bond is not involved in too many hydrogen bonds. EPR spectral simulations indicate that there potentially is g-strain in the x-direction (Figure 1b), indicating that statistically seen there will be some molecules that are hydrogen bonded along N−O⋯H−OH, but by summation over the small amount of selected orientations, this small number of H-bonded molecules is not enough to notably contribute to an ENDOR signal. This result also manifests itself in the MD simulations. The coordination number for the nitroxide group is much smaller than for the sulfonate groups, showing less hydrogen bonds along the molecular x-axis. When inspecting the low-field region of the ESE-detected EPR spectra of the different samples, we only observed a shift of the g_{xx}-value in the water-rich solvent mixture with 70 vol % water. Due to the smaller size of water compared to methanol, it may approach the NO group closer, and the hydrogen-bonding capability is much higher for water. The other two solvent compositions (50 and 70 vol % MeOH) show no shifts, which indicates that the hydrogen bonding to NO is similar in both.

The respective methyl proton splittings in the solvent mixtures show the same features for Mims (Figure 3a) and Davies (Figure 4b) ENDOR measurements. Here, two smaller hfc's are found at each molecular orientation and are assigned to more distant methanol molecules for which and we cannot get distance orientation information. From the largest hfc, which arises along the molecular z-axis (parallel to the SOMO) and can be simulated as being purely anisotropic, a distance of 3.5 ± 0.1 Å can be extracted. Thus, methyl protons approach closest from "bottom" and "top" of the FS molecule's (approximate) plane spanned by O−N−(S)$_2$.

Using a sum of the proton "densities" from an ensemble of snapshots from the MD simulations, one can not only visualize but also understand the results of the MD simulations and the ENDOR experiments (Figure 5a) and draw a molecular picture of the solvation around FS. Figure 5b shows the chemically different types of protons around the probe molecule (hydrophobic methyl protons, green; exchangeable protons from water and the hydroxyl groups, cyan). The shortest distance for methyl protons is found to be 2.8 Å along the long axis of the SOMO (Figure 1a). The ENDOR experiments were performed at 20 K, where methyl group rotation is still active[65] and the three equivalent protons contribute to a (hypothetical) averaged ^{1}H signal. Taking a CH bond length of 1.093 Å and a HCH angle of 109.3°,[66] one can calculate that the distance from the center of the NO group to the "averaged" proton is 1.03 Å longer than the distance to the closest proton (assuming that this closest proton is pointing toward the NO group). Since in pulse ENDOR experiments at 20 K one measures an averaged proton−electron distance and setting the closest proton−electron distance to 2.8 Å, as found by MD simulation, one gets an averaged distance of 3.8 ± 0.1 Å for the experiments, which is—considering the broad ensemble of solvation situations—in good agreement with the 3.5 Å found from the simplified calculation from the ENDOR experiments. We refrain from assigning a "true" proton−electron distance since the underlying one has the complicated situation that there is a distribution of hf couplings that are weighted by $1/r^3$ and these hyperfine responses are further weighted by either the Mims or Davies ENDOR response functions.

The preferential arrangement of the methyl groups above and below the NO bond is due to two forces: First, in this way the strong H-bonded network around the two sulfonate groups (as seen in the MD simulations) is less disturbed. Methanol can

act as one H-bond donor, and if the methanol−OH group is H-bonded to one of the highly hydrophilic sulfonate groups, placing the methyl group at the sulfonate group (and hence reducing the number of H-bonds) would be energetically unfavorable. The second argument is of steric nature. The largest "free" space for the (in relation to any other components in the solvent mixtures) bulky methyl groups is simply given at these positions of the molecule due to the sulfonate groups. Thus, this specific solvation situation is found to be due to an interplay between electrostatic, hydrogen-bonding, and steric effects.

The microheterogeneity of the binary solvent structure without solute molecules can be assumed to be highly similar in all our cases, as proposed by Zhao et al.[67] All our tested methanol molar ratios are in a composition region, in which methanol−water associates of one molecule of methanol with two molecules of water have been observed by IR.[67] When considering our experimental findings, this indicates that also in the case with solute molecules the same solvation characteristics are found for all volume ratios studied here. This, in turn, suggests that in a broad range of compositions the solute molecules FS (or many of them, at least) "force" the water and methanol molecules into a solvation shell that resembles the one found in our study and depicted in Figure 5b.

5. Conclusions and Outlook

The molecular picture of the solvation around Fremy's salt in a 50:50 (v/v) mixture of methanol and water, which is derived from the MD simulations, is in full agreement with our ENDOR results and is summarized in Figure 5b. Both exchangeable species (water and hydroxyl protons) are able to establish hydrogen bonds to the FS dianion with an angular distribution that reflects the sterical hindrance of the NO hydrogen-bond acceptor site by the sulfonate groups. Hence, exchangeable protons come in closest contact with the NO moiety along the molecular y-axis of the probe molecule. If the methanol−OH group (instead of water) is hydrogen bonded to the sulfonate groups, it is energetically favorable to *not* place the methyl group at the sulfonate group, as this would disturb the existing H-bond network and reduce the number of H-bonds. It is thus favorable to place the methyl groups on the "top" and "bottom" of the (approximate) plane spanned by O−N−(S)$_2$. Also, the largest "free" space for the methyl groups is given at these positions of the molecule due to the sulfonate groups. Thus, the preferential arrangement of methyl groups along the molecular z-direction of the nitroxide can be explained by the interplay of *electrostatic and hydrogen-bonding* (H-bonds around sulfonate groups) and *steric* (bulky methyl group) effects.

The elucidation of the microscopic solvation of a small probe molecule in binary solvent mixtures represents the first step for understanding the interactions in more complex biochemical systems. In particular, this includes the potential perturbation of the H-bond network due to the presence of a spin probe.

Further work on variable mixing time (VMT) ENDOR[68,69] is in progress to get information about the sign of the hyperfine coupling, which is important for the unambiguous determination of the isotropic and anisotropic parts of the interaction, and the approach will be extended to other solvents and solute molecules.

References and Notes

(1) Reichardt, C. *Solvents and Solvent Effects in Organic Chemistry*, 2nd ed.; VCH: Weinheim, 1988.

(2) Bagotsky, S. *Fundamentals of Electrochemistry*, 2nd ed.; Wiley-Interscience: NJ, 2006.

(3) Marcus, Y. *Solvent Mixtures Properties and Selective Solvation*; Marcel Dekker: Basel, 2002.

(4) Ben-Naim, A. *J. Phys. Chem.* **1989**, *93*, 3809–3813.

(5) Wahab, A.; Mahiuddin, S. *J. Solution Chem.* **2005**, *34*, 537–560.

(6) Chatterjee, P.; Bagchi, S. *J. Chem. Soc., Faraday Trans.* **1990**, *86*, 1785–1789.

(7) Hefter, G. *Pure Appl. Chem.* **2005**, *77*, 605–617.

(8) Hawlicka, E.; Swiatla-Wojcik, D. *Chem. Phys.* **1995**, *195*, 221–233.

(9) Bujnicka, K.; Hawlicka, E. *J. Mol. Liq.* **2006**, *125*, 151–157.

(10) Sakurai, M.; Yoshimori, A. *Chem. Phys. Lett.* **2003**, *371*, 23–28.

(11) Tongraar, A.; Rode, B. M. *Phys. Chem. Chem. Phys.* **2004**, *6*, 411–416.

(12) Attanasio, D. *J. Phys. Chem.* **1986**, *90*, 4952–4957.

(13) Mustafi, D.; Makinen, M. W. *Inorg. Chem.* **1988**, *27*, 3360–3368.

(14) van Willigen, H. *Chem. Phys. Lett.* **1979**, *65*, 490–493.

(15) van Willigen, H. *J. Magn. Reson.* **1980**, *39*, 37–46.

(16) Feher, G. *Phys. Rev.* **1956**, *103*, 834.

(17) Steinhoff, H.-J.; Savitsky, A.; Wegener, C.; et al. *Biochim. Biophys. Acta, Bioenerg,* **2000**, *1457*, 253–262.

(18) Steinhoff, H.-J. *Biol. Chem.* **2005**, *385*, 913–920.

(19) Weil, J. A.; Bolton, J. R.; Wertz, J. E. *Electron Paramagnetic Resonance*; Wiley: New York, 1994.

(20) Bales, B. L.; Wajnberg, E.; Nascimento, O. R. *J. Magn. Reson., Ser. A* **1996**, *118*, 227–233.

(21) Zielonka, J.; Zhao, H.; Xu, Y.; et al. *Free Radical Biol. Med.* **2005**, *39*, 853–863.

(22) Liu, Z.-L.; Han, Z.-X.; Chen, P.; et al. *Chem. Phys. Lipids* **1990**, *56*, 73–80.

(23) Hinderberger, D.; Spiess, H. W.; Jeschke, G. *Europhys. Lett.* **2005**, *70*, 102–108.

(24) Hinderberger, D.; Spiess, H. W.; Jeschke, G. *J. Phys. Chem. B* **2004**, *108*, 3698–3704.

(25) Hinderberger, D.; Schmelz, O.; Rehahn, M.; et al. *Angew. Chem.* **2004**, *116*, 4716–4721.

(26) Prandolini, M. J.; Denysenkov, V. P.; Gafurov, M.; et al. *J. Am. Chem. Soc.* **2009**, *131*, 6090–6092.

(27) Nayak, S. P.; Gowda, B. T. *J. Phys. Org. Chem.* **1992**, *5*, 755–763.

(28) Mims, W. B. *Proc. R. Soc. (London), Ser. A* **1965**, *283*, 452–457.

(29) Davies, E. R. *Phys. Lett. A* **1974**, *47*, 1–2.

(30) Kuharski, R. A.; Rossky, P. J. *J. Chem. Phys.* **1985**, *82*, 5164–5177.

(31) Tomberli, B.; Egelstaff, P. A.; Benmore, C. J.; et al. *J. Phys. Condens. Matter* **2001**, *13*, 11421–11434.

(32) Moser, W.; Howie, R. A. *J. Chem. Soc. A* **1986**, 3039–3043.

(33) Wilson, B. J.; Ritter, D. M. *Inorg. Chem.* **1963**, *2*, 974–978.

(34) Wilson, B. J.; Hayes, J. M.; Durbin, J. A. *Inorg. Chem.* **1976**, *15*, 1702–1704.

(35) Goldman, S. A.; Bruno, G. V.; Freed, J. H. *J. Chem. Phys.* **1973**, *59*, 3071–3091.

(36) Goldman, S. A.; Bruno, G. V.; Polnaszek, C. F.; et al. *J. Chem. Phys.* **1972**, *56*, 716–735.

(37) Atherton, N. M.; Brustolon, M. *Mol. Phys.* **1976**, *32*, 23–31.

(38) Mikhail, S. Z.; Kimel, W. R. *J. Chem. Eng. Data* **1961**, *6*, 533–537.

(39) Static Dielectric Constants of Pure Liquids and Binary Liquid Mixtures. In *Landolt-Börnstein - Group IV Physical Chemistry Numerical Data and Functional Relationships in Science and Technology*; Landolt-Börnstein, Ed.; Springer: Berlin Heidelberg; Vol. 17, 2008.

(40) Smirnova, T. I.; Smirnov, A. I. High-Field ESR Spectroscopy in Membrane and Protein Biophysics. In *Biological Magnetic Resonance*; Hemminga, M. A., Berliner, L. J., Eds.; Springer: New York, 2007; Vol. 27, pp 165−251.

(41) Makinen, M. W. *Spectrochim. Acta, Part A* **1998**, *54*, 2269–2281.

(42) Rist, G. H.; Hyde, J. S. *J. Chem. Phys.* **1970**, *52*, 4633–4643.

(43) Hoffman, B. M.; Ronald, A. V.; Martinsen, J. *J. Magn. Reson.* **1985**, *62*, 537–542.

(44) Hoffman, B. M.; Ronald, A. V.; Martinsen, J. *J. Magn. Reson.* **1984**, *59*, 110–123.

(45) Schweiger, A.; Jeschke, G. *Principles of Pulse Electron Paramagnetic Resonance*; Oxford University Press: New York, 2001.

(46) Stoll, S.; Schweiger, A. *J. Magn. Reson.* **2006**, *178*, 42–55.

(47) Hess, B.; Kutzner, C.; van der Spoel, D.; et al. *J. Chem. Theory Comput.* **2008**, *4*, 435.

(48) Nosé, S. *Mol. Phys.* **1984**, *52*, 255.

(49) Hoover, W. G. *Phys. Rev. A* **1985**, *31*, 1695.

(50) Darden, T.; York, D.; Pederse, L. *J. Chem. Phys.* **1993**, *98*, 10089.

(51) Essmann, U.; Perera, L.; Berkowitz, M. L.; et al. *J. Chem. Phys.* **1995**, *103*, 8577.

(52) Jorgensen, W. L.; Maxwell, D. S.; Tirado-Rives, J. *J. Am. Chem. Soc.* **1996**, *118*, 11225.

(53) Jorgensen, W. L.; Chandrasekhar, J.; Madura, J. D. *J. Chem. Phys.* **1983**, *79*, 926.

(54) Frisch, M. J.; Trucks, G. W.; Schlegel, H. B.; Scuseria, G. E.; Robb, M. A.; Cheeseman, J. R.; Montgomery, J. A., Jr.; Vreven, T.; Kudin, K. N.; Burant, J. C.; Millam, J. M.; Iyengar, S. S.; Tomasi, J.; Barone, V.; Mennucci, B.; Cossi, M.; Scalmani, G.; Rega, N.; Petersson, G. A.; Nakatsuji, H.; Hada, M.; Ehara, M.; Toyota, K.; Fukuda, R.; Hasegawa, J.; Ishida, M.; Nakajima, T.; Honda, Y.; Kitao, O.; Nakai, H.; Klene, M.; Li, X.; Knox, J. E.; Hratchian, H. P.; Cross, J. B.; Bakken, V.; Adamo, C.; Jaramillo, J.; Gomperts, R.; Stratmann, R. E.; Yazyev, O.; Austin, A. J.; Cammi, R.; Pomelli, C.; Ochterski, J. W.; Ayala, P. Y.; Morokuma, K.; Voth, G. A.; Salvador, P.; Dannenberg, J. J.; Zakrzewski, V. G.; Dapprich, S.; Daniels, A. D.; Strain, M. C.; Farkas, O.; Malick, D. K.; Rabuck, A. D.; Raghavachari, K.; Foresman, J. B.; Ortiz, J. V.; Cui, Q.; Baboul, A. G.; Clifford, S.; Cioslowski, J.; Stefanov, B. B.; Liu, G.; Liashenko, A.; Piskorz, P.; Komaromi, I.; Martin, R. L.; Fox, D. J.; Keith, T.; Al-Laham, M. A.; Peng, C. Y.; Nanayakkara, A.; Challacombe, M.; Gill, P. M. W.; Johnson, B.; Chen, W.; Wong, M. W.; Gonzalez, C.; Pople, J. A. *Gaussian 03*, revision C.02; Gaussian, Inc.: Wallingford, CT, 2004.

(55) Bayly, C. I.; Cieplak, P.; Cornell, W.; et al. *J. Phys. Chem.* **1993**, *97*, 10269–10280.

(56) Astashkin, A. V.; Kawamori, A. *J. Magn. Reson.* **1998**, *135*, 406–417.

(57) Epel, B.; Pöppl, A.; Manikandan, P.; et al. *J. Magn. Reson.* **2001**, *148*, 388–397.

(58) Howie, R. A.; Glasser, L. S. D.; Moser, W. *J. Chem. Soc. A* **1986**, 3043–3047.

(59) Erickson, R. *J. Chem. Phys.* **1996**, *202*, 263−275.

(60) Morrone, J. A.; Car, R. *Phys. Rev. Lett.* **2008**, *101*, 017801.

(61) Chen, B.; Ivanov, I.; Klein, M. L.; et al. *Phys. Rev. Lett.* **2003**, *91*, 215503.

(62) Marx, D.; Tuckerman, M. E.; Parrinello, M. *J. Phys. Condens. Matter* **2000**, *12*, A153–A159.

(63) Morrone, J. A.; Srinivasan, V.; Sebastiani, D.; et al. *J. Chem. Phys.* **2007**, *126*, 234504–9.

(64) Hayes, R. L.; Paddison, S. J.; Tuckerman, M. E. *J. Phys. Chem. B* **2009**, *113*, 16574–16589.

(65) McBrierty, V. J. *Polymer* **1974**, *15*, 503–520.

(66) Ivash, E. V.; Dennison, D. M. *J. Chem. Phys.* **1953**, *21*, 1804–1816.

(67) Zhao, Z.; Malinowski, E. R. *Anal. Chem.* **1998**, *71*, 602–608.

(68) Bennebroek, M. T.; Schmidt, J. *J. Magn. Reson.* **1997**, *128*, 199–206.

(69) Epel, B.; Manikandan, P.; Kroneck, P.; et al. *Appl. Magn. Reson.* **2001**, *21*, 287–297.